Path-integral Monte Carlo study of a model two-dimensional quantum paraelectric

R. Martoňák and E. Tosatti*
International School for Advanced Studies, Via Beirut 2–4, 34014 Trieste, Italy
(Received 21 June 1993; revised manuscript received 29 November 1993)

We have started a study of quantum ferroelectrics and paraelectrics. Simple two-dimensional short-range lattice model Hamiltonians are constructed, keeping in mind the phenomenology of real perovskite systems, like $SrTiO_3$ and $KTaO_3$. Pertinent quantum tunneling phenomena, and the presence of an icelike constraint are demonstrated. The two simplest models, namely a plain quantum four-state clock model and a constrained one, are then studied in some detail. We show the equivalence of the former, but not of the latter, to a quantum Ising model. For the latter, we describe a very good analytical wave function valid in the special case of zero coupling ($J = 0$). In order to study the full quantum statistical mechanics of these models, a path-integral Monte Carlo calculation is set up, and implemented with a technique, which even in the constrained case permits a good convergence for increasing time slice number m. The method is applied first to the unconstrained model, which serves as a check, and successively to the constrained quantum four-state clock model. It is found that in both cases a quantum phase transition at $T = 0$ takes place at finite coupling J, between a ferroelectric and a quantum paraelectric state, even when the constraint hinders disordering of the ferroelectric state. These model paraelectric states have a finite excitation gap, and no broken symmetry. The possible role of additional ("oxygen hopping") kinetic terms in making closer contact with the known phenomenology of $SrTiO_3$ is proposed.

I. INTRODUCTION

It is well known that large enough quantum fluctuations can destabilize the ferroelectric state in favor of a paraelectric state, which possesses no net polarization order parameter even at zero temperature.[1] Unlike classical paraelectrics, where disorder is temperature induced, quantum paraelectrics (QPE) are in a sense very much ordered, in that their ground state corresponds to a well-defined wave function encompassing all dipoles in the macroscopic system. This aspect makes them especially interesting, also in connection with a recent suggestion[2] that some kind of macroscopic coherence, or off-diagonal long-range order (ODLRO), might appear under special circumstances.

Three-dimensional (3D) examples of quantum paraelectric states are believed to be provided, among others, by the low-temperature states of $SrTiO_3$,[1–3] $KTaO_3$,[4] as well as KH_2PO_4 above 16.6 kbar.[5] In these systems, quantum fluctuations suppress ferroelectricity, characterized by an n-component real order parameter ($n = 2$ in tetragonal $SrTiO_3$, $n = 3$ in cubic $KTaO_3$, $n = 1$ in KH_2PO_4).

Interest in quantum ferroelectrics started in the late 1950s,[6] and revived again in the late 1970s,[1] at a time when attention was focused on critical exponents of the quantum phase transition, including the crossover between quantum and classical critical exponents.[7–9] It has continued more recently, with impurity-induced transitions from quantum paraelectric to domain-type ferroelectric.[10–12] Apart from that, there seems to exist no real attempt as yet to study the nature of the quantum-mechanical state of QPE's in a well-defined realization.

Our goal with this paper is to begin a microscopic study of models which exhibit quantum ferroelectric and quantum paraelectric behavior. The method we will apply is a mixture of variational, mean-field theory, and principally the path-integral Monte Carlo (PIMC) method, coupled when possible with finite size scaling.[13]

The first, and main problem, is the choice of an appropriate model Hamiltonian. In choosing the model, we try to adhere as much as possible to the actual physical situation of $SrTiO_3$, whose phenomenology seems best known. However, a drastic amount of simplification is clearly needed. On the one hand, the real crystal is rich in complications, such as coupling to antiferrodistortive and to elastic degrees of freedom.[14] On the other hand, even if the PIMC method is a powerful tool for quantum statistical mechanics, the system one can hope to study with the present means is by necessity very simple and relatively small sized. Our first step, therefore, must be a judicious choice of the main ingredients of the problem. We can be guided, first of all, by the existing understanding of classical ferroelectrics.

The plan of this paper is as follows. In Sec. II we first briefly review the phenomenology of quantum paraelectrics, with emphasis on the crossover from the displacive to the order-disorder regime. After demonstrating the relevance of the four-state clock model in the case of $SrTiO_3$, we discuss in detail various possible quantum effects, as well as the presence of several important constraints. In Sec. III we then consider the simple (unconstrained) quantum four-state clock model. Its general equivalence to two uncoupled Ising models, already known classically, will be proved for the quantum case as well. In Sec. IV, we add a constraint to the quantum four-state clock model, and discuss a simple approximate

wave function for the case of zero temperature and zero coupling. Section V introduces the technicalities of our PIMC calculation. In order to treat the constraint properly and preserve the usual $1/m^2$ convergence in the number of Trotter slices, we introduce a particular version of the checkerboard decomposition scheme, commonly used, e.g., for simulation of quantum spin systems.[15] Section VI presents a PIMC test study of the simple quantum four-state clock model. Comparison with the known results of the quantum Ising model, done throughout that section, serves as a check of the basic soundness of the PIMC method, as well as of the kind of errors to be expected in later applications. In Sec. VII the PIMC method is applied to the *constrained* four-state clock model. It is found, as expected, that for given values of quantum hopping and coupling constant, the ferroelectricity is now stronger, and the ferro-para transition occurs at substantially higher temperature in the constrained case than in the unconstrained case. In spite of this strengthening of the ferroelectricity, there still is a critical value of the coupling constant, below which the system is a quantum paraelectric at $T = 0$. However, this critical value is now a factor of ~ 4 smaller, due to the constraint. Finally, Sec. VIII is devoted to a general discussion and relevance of the present results to the known phenomenology of the perovskite QPE's. In particular, the $T = 0$ state of both models studied so far does not exhibit in the QPE regime any broken symmetry or ODLRO, and can be reached from the high-temperature paraelectric state without a phase transition. Therefore, the question of understanding the phase transition described by Ref. 2 is left open.

II. CHOICE OF MODELS

Microscopic models for classical ferroelectricity have been available for a long time.[16] Among them, very popular are soft-mode lattice-dynamical models,[17] and ice models.[18] Ferroelectricity, in fact, represents just a particular case of a more general class of phenomena, that of *structural phase transitions.* An extensive and definitive review of critical phenomena related to *classical* structural transitions has been provided in Ref. 16. Here we concentrate on some pertinent points, concerning the phenomenology of the *quantum* paraelectrics.

At high enough temperature, the quantum perovskites $SrTiO_3$, $KTaO_3$ become just ordinary classical paraelectrics, well described by the displacive limit. This classical displacive behavior is confirmed by neutron and Raman spectra showing very well-defined optically active TO modes, hard and narrow. These modes soften down upon cooling, as expected in the displacive picture.[19] However, just above the *extrapolated classical* Curie temperature T^* (37 K for $SrTiO_3$, 40 K for $KTaO_3$), the picture changes. In $SrTiO_3$, the enhanced anomalous hyper-Rayleigh scattering[20] indicates the presence of local disorder, or off-center displacement of the ions, which locally breaks the inversion symmetry. Various anomalies observed in the spectroscopy of soft and acoustic modes in $SrTiO_3$ (Ref. 21) point to the existence of large clusters, whose typical size is roughly equal to the reciprocal of the reduced wave vector for which the anomalies are most pronounced, i.e., $\xi^{-1} = 0.04^{-1} \sim 20$ lattice constants at very low T. In $KTaO_3$, NMR data of Rod, Borsa, and van der Klink[11] clearly indicate an off-center displacement of Ta ions which sets up rather abruptly below $T^* \sim 40$ K. In the microwave region, the slow Debye relaxations typical of the order-disorder regime appear in $KTaO_3$, their typical frequency τ^{-1} again decreasing with temperature.[22] These are the usual signals of crossover into the critical, order-disorder regime of ordinary classical paraelectrics. *This crossover therefore takes place also in the QPE perovskites.* Unlike the classical systems, however, in this case the critical slowing down, i.e., the divergence of τ with decreasing T, appears to be blocked at some *finite* relaxation time τ^*, which in $KTaO_3$ is very long, $(\tau^*)^{-1} <\sim 500$ MHz.[22] Because of this lack of divergence of τ, long-range ferroelectric order is never reached, and the system remains paraelectric even at the lowest temperatures. The failure to order ferroelectrically accompanied by these slow dielectric fluctuations has been attributed to quantum zero-point motion.[1] There is clear evidence showing that fluctuations can be easily removed, the system correspondingly turning into a regular ordered ferroelectric, by applying either pressure[14] or impurity doping.[10] We conclude that when approaching T^* from above, the QPE perovskites are well inside the order-disorder regime. A sort of quantum order-disorder regime appears moreover to persist all the way down to $T = 0$. Between T^* and $T = 0$, we have a sort of "quantum central peak" state — rather than completing its classical slowing down, and undergoing a regular ferroelectric critical point transition, the system hangs indefinitely on the verge of criticality, due to quantum fluctuations.

An important corollary of this discussion is that a discrete lattice model, which lends itself better to a description of order-disorder critical fluctuations, is more likely to yield, probably even in the details, a better description of the QPE state, rather than a continuous, displacive model.

The paradigmatic *discrete* model for quantum paraelectricity with a scalar order parameter is the Ising model in transverse field.[23,24] Its relevance is particularly direct for the description of hydrogen-bonded ferroelectrics, like KH_2PO_4. The order parameters in $KTaO_3$ and $SrTiO_3$ are not exactly Ising like, however. $KTaO_3$ remains cubic down to the lowest temperatures and the order parameter has thus three components. $SrTiO_3$, which acquires a tetragonal structure at low temperatures (below 105 K), can become ferroelectric when doped by Ca and the resulting ferroelectricity is known to be XY like.[10] In pure $SrTiO_3$, in particular, if the tetragonal axis z is taken along [001], so that below 105 K two neighboring TiO_3 octahedra rotate by an angle Φ and $-\Phi$ around z ($\langle\Phi\rangle \simeq 5°$ well below 105 K), then ferroelectricity shows a tendency to occur along either $\pm$[100] or $\pm$[010], and more generally in the (001) XY plane. In the ferroelectric state, the central ion Ti establishes a *slightly stronger* bond with one of the four coplanar oxygens (which surround it in the XY plane), than

with the other three. Coupling between different cells is not exclusively dipole-dipole, but should have important electronic contributions (short range), and elastic contributions (long range). The elastic coupling mechanism, in particular, is likely to be very strong, as confirmed by the fact that even a small pressure along x is sufficient to yield ferroelectric order along y.[14] Physically, what we believe happens is that a double-well situation for the central Ti ion (or equivalently for a bridging oxygen between two Ti ions), say, along [100], can occur only if the lattice is *locally* expanded along that direction (spontaneously or due to an external factor). Some of the consequences of the coupling of ferroelectricity to elastic modes, leading in particular to incommensurability phenomena, and the possible role of quantum effects have been given a separate discussion elsewhere.[26]

In the present lattice modeling, we shall however ignore these details, and assume simply a short-range ferroelectric coupling J, between first neighbor cells. Each cell has an XY phase variable ϕ, representing the Ti displacement, or the dipole direction, subject to a cubic anisotropy, with minima at $\phi = 0, \pm\pi/2, \pi$. In the large anisotropy limit, a minimal lattice model of ferroelectricity in $SrTiO_3$ is therefore a 3D four-state clock model with first neighbor coupling. This leaves entirely out possible long-range effects due to dipole-dipole coupling, and to coupling to elastic modes, as mentioned above, as well as additional coupling to the antiferrodistortive order parameter. In order to make quantitative progress, we choose to ignore all these complications for the time being, even though they will probably have to be reconsidered at a later stage.

By introducing at each site a complex variable

$$z_i = e^{i\phi_i} , \tag{1}$$

where ϕ_i can take the four values $0, \pm\pi/2, \pi$, the ordinary, classical four-state clock model can be written as

$$H^4 = \sum_i H_i^4 , \tag{2}$$

$$H_i^4 = -\frac{J}{2}\sum_j \cos(\phi_i - \phi_j) = -\frac{J}{2}\mathrm{Re}\left(\sum_j z_i z_j^*\right) ,$$

where the sum over j runs over nearest neighbors of i.

It was shown by Suzuki[27] that the classical four-state clock model is mapped in full generality, i.e., independently both of dimensionality and of range of interaction, onto two decoupled Ising models. Hence, everything is known about the classical behavior of model (2).

However, we must now introduce quantum-mechanical effects, in the form of a kinetic energy term, not commuting with the potential energy (2). In a perovskite ferroelectric, one can envisage at least two distinct quantum effects, both resulting in dipole tunneling.

The first is quantum hopping of the central positive ion (which will be called Ti, since it is Ti in $SrTiO_3$), from bonding preferentially one oxygen to bonding the next one, within the same cage, or cell [Fig. 1(a)]. The kinetic energy for this is, in the continuous case,

$$H^{\mathrm{kin}\,1} = \frac{\mu\rho^2}{2}\sum_j \dot{\phi}_j^2 = \frac{1}{2\mu\rho^2}\sum_j \left(-i\hbar\frac{\partial}{\partial\phi_j}\right)^2 , \tag{3}$$

where μ and ρ are effective mass and off-center displacement [a very small quantity, of order of 0.03 Å (Ref. 1)] of the Ti ion. In our discrete case, we shall allow the clock variable z_j to hop, for simplicity, into its two nearest orientations, i.e., from z_j into $\pm i z_j$. If we choose to describe the system with a wave function $\Psi(z_1, \ldots, z_n)$, the corresponding kinetic piece of the Hamiltonian reads

$$H^{\mathrm{kin}\,1} = \sum_j H_j^{\mathrm{kin}\,1} ,$$

$$H_j^{\mathrm{kin}\,1}\Psi(z_1, \ldots, z_j, \ldots, z_n) = -t[\Psi(z_1, \ldots, iz_j, \ldots, z_n) + \Psi(z_1, \ldots, -iz_j, \ldots, z_n)] . \tag{4}$$

In the last expression, the hopping energy has further been lumped into the constant $t = \frac{\hbar^2}{2\mu\rho^2}$. This term is an obvious generalization of the "transverse field" term in the Ising case. If strong enough, it will cause the dipole in each cell to hop quantum mechanically from one value of ϕ_j to the other, irrespective of the state of dipoles in neighboring cells, thereby destroying ferroelectric long-range order.

A second type of quantum effect, which has apparently not been discussed so far, is *oxygen double-well tunneling*. When an oxygen is bonded to a given Ti ion, we can imagine another energy minimum, more or less equivalent, when that oxygen is bonded to the other Ti ion on the opposite side [Fig. 1(b)]. Quantum hopping processes of the oxygen between these two sites (similar to proton hopping in hydrogen bonds) may play a role in quantum paraelectrics, both because of a relatively small displacement involved and of the small oxygen mass. However, these processes cause the bond to hop from one cage to the next and therefore, unlike the intracage hopping (4), they do not obey the (apparently sensible) requirement that the number of bonds per cage should not exceed 1. An adequate prescription is thus necessary to include the oxygen tunneling into our scheme.

We have envisaged so far two possible implementations of oxygen tunneling. The first is one where we force each cage to retain *one and only one dipole bond* in any given configuration. The second is a different scheme, where we introduce the possibility of "bond vacancies," while still forbidding double bond occupancy of any cage. We discuss both schemes in this order.

If each cage is constrained to retain strictly one and only one bond at any given time, bond hopping becomes extremely problematic. For each bond which hops, a

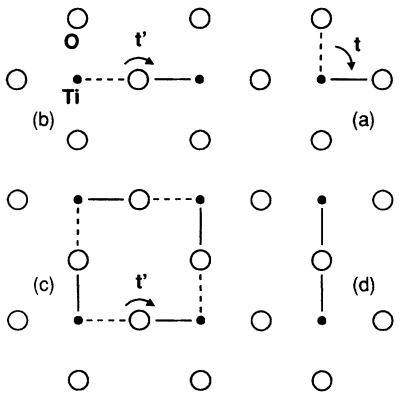

FIG. 1. A square lattice of oxygen cages with Ti ions inside. (a) Intracage bond hopping, corresponding to kinetic energy $H^{\text{kin 1}}$ (4). (b) Intercage bond hopping, due to oxygen tunneling, corresponding to kinetic energy $H^{\text{kin 2a}}$ (6), and $H^{\text{kin 2b}}$ (8). (c) The simplest concerted bond hopping mechanism, taking place on the elementary plaquette. (d) A forbidden configuration, with two bonds sharing the same bridging oxygen.

suitable "bond backflow" loop is mandatory, so as to obey the one-bond-per-cage constraint everywhere. In other words, only *concerted rearrangements*, such as ring-shaped currents of bonds, are permitted. The simplest concerted bond hopping loop is shown in Fig. 1(c). The associated kinetic energy is a sum of four-body operators over plaquettes,

$$H^{\text{kin 2a}} = \sum_{\text{plaquettes}} H_i^{\text{kin 2}a}, \tag{5}$$

which can be symbolically written as

$$H_i^{\text{kin 2}a} = -t'\left\{\left|\begin{matrix}\rightarrow & \downarrow \\ \uparrow & \leftarrow\end{matrix}\right\rangle\left\langle\begin{matrix}\downarrow & \leftarrow \\ \rightarrow & \uparrow\end{matrix}\right| + \left|\begin{matrix}\downarrow & \leftarrow \\ \rightarrow & \uparrow\end{matrix}\right\rangle\left\langle\begin{matrix}\rightarrow & \downarrow \\ \uparrow & \leftarrow\end{matrix}\right|\right\}. \tag{6}$$

In process (6), concerted ring bond hopping can take place only on plaquettes, around closed loops [Fig. 1(c)]. Also, it is ineffective if the initial state is a fully aligned ferroelectric. More general concerted processes should also be interesting, and do not necessarily have this limitation. However, we do not wish to go into this discussion at this stage.

The second possibility is a scheme in which we still forbid multiple bond occupancy of a cage, but we allow for the possibility of *bond vacancies*, i.e., cages where the Ti ion is centrally located (or else it moves out of plane), so that it has no in-plane dipole bond at all. The justification for this comes from the necessity to include at temperatures close to and higher than T^*, elements which link the present discrete model with the displacive picture, eventually applicable when $T \gg T^*$. At these high temperatures, the likeliest Ti ion location is indeed the cage center, and there are physically no more bonds to speak of. Introduction of some bond vacancies even at lower temperatures allows for a *new* bond hopping process, where a vacancy in one cage and a bond in a neighboring cage can exchange positions. The link oxygen between two cages can "resonate" between two adjacent Ti ions, both of which are free from other bonds. The corresponding piece of Hamiltonian is now a sum of two-body operators,

$$H^{\text{kin 2}b} = \sum_{\langle ij \rangle} H_{ij}^{\text{kin 2}b}. \tag{7}$$

These can be written symbolically, e.g., for a horizontal link, $\langle i, j = i + \mathbf{x} \rangle$, as

$$H_{ij}^{\text{kin 2}b} = -t'\left(|\rightarrow_i, \circ_j\rangle\langle\circ_i, \leftarrow_j| + |\circ_i, \leftarrow_j\rangle\langle\rightarrow_i, \circ_j|\right), \tag{8}$$

and analogously for a vertical link, where the symbol $\circ_i$ denotes a bond vacancy on site i. Through processes (8), vacancies and bonds become mobile, and the possibility of condensates may arise at sufficiently low temperatures.

In this initial paper, we will restrict ourselves to consider only the on-site kinetic energy (4), as a first step. Dealing with processes of the type (6) or (8) is evidently more complex, and we defer that until after obtaining a good understanding of the more basic terms.

Besides potential and kinetic energies, we have also found that the problem of ferroelectricity (both classical and quantum) in a perovskite requires a third, novel ingredient. That ingredient is an anholonomic *constraint*, which in Hamiltonian terms can be mimicked by some *infinite* repulsion or attraction. The physical constraint we consider is that *no oxygen* should be bound (i.e., form a dipole) *simultaneously* to both Ti atoms on the two sides of the link where it belongs. In other words, while a Ti atom has always one and only one bond (barring bond vacancies from now on), an O atom can have either zero or one bond, but not two: The configuration of Fig. 1(d) is physically meaningless, and should not occur. The constraint can also be included as a Hamiltonian term, in the following way. First we introduce for each link an operator

$$P'_{ij} = \delta(z_i - r_{ij})\delta(z_j + r_{ij}), \tag{9}$$

which acts as a projector on the forbidden states. In this expression, $r_{ij} = r_j - r_i$, where r_i is the complex number defining the 2D position of site i. The Hamiltonian term equivalent to the constraint then reads

$$H^{\text{constr}} = \lim_{U \to \infty} U \sum_{\langle ij \rangle} P'_{ij}. \tag{10}$$

Enforcement of this constraint is analogous to an "ice rule" and has also apparently never been considered before for the perovskites or any displacive ferroelectric. It is likely to yield nontrivial modifications in the physics. At the classical level, for example, we expect a dramatic reduction of entropy due to the decreased number of available configurations, and a possible change of the critical point universality class. Related effects are expected in the quantum paraelectric problem, which is of direct interest to us.

Finally, we have to choose dimensionality. While the physical system is of course in 3D, we see no major harm in restricting our study to a 2D square lattice of cages.

This amounts to treating, so to speak, a single TiO_2 plane, ignoring interplanar coupling. This seems a particularly plausible approximation in the case of $SrTiO_3$, where ferroelectric Ti-O bonds are mostly planar, and do not involve the interplanar bridging oxygens.

III. SIMPLE QUANTUM FOUR-STATE CLOCK MODEL

In this section we shall consider the simplest of the models, which is defined by the Hamiltonian

$$H = H^4 + H^{\text{kin}\,1} = \sum_j H_j^4 + \sum_j H_j^{\text{kin}\,1} . \tag{11}$$

This model can be mapped on two *decoupled* Ising models in a transverse field, regardless of dimensionality. In order to construct the mapping, it is convenient to start from the ϕ_i representation.

We represent the clock variable ϕ_i on each site by two discrete variables s_i and σ_i, defined respectively by

$$s_i = \sqrt{2}\cos\left(\phi_i + \frac{\pi}{4}\right) ,$$
$$\sigma_i = \sqrt{2}\sin\left(\phi_i + \frac{\pi}{4}\right) . \tag{12}$$

It is easily seen that $s_i, \sigma_i = \pm 1$, and thus the new variables can be regarded as Ising variables. The potential energy term can be immediately written as

$$H_i^4 = -\frac{J}{2}\sum_j \cos(\phi_i - \phi_j) = -\frac{\frac{1}{2}J}{2}\sum_j (s_i s_j + \sigma_i \sigma_j) , \tag{13}$$

which is just Suzuki's classical decoupling.[27]

The kinetic energy term can be written as

$$\begin{aligned} H_i^{\text{kin}\,1}\Psi(s_1,\sigma_1;\ldots;s_i,\sigma_i;\ldots;s_n,\sigma_n) &= H_i^{\text{kin}\,1}\Psi(\phi_1,\ldots,\phi_i,\ldots,\phi_n) \\ &= -t\left[\Psi(\phi_1,\ldots,\phi_i-\frac{\pi}{2},\ldots,\phi_n) + \Psi(\phi_1,\ldots,\phi_i+\frac{\pi}{2},\ldots,\phi_n)\right] \\ &= -t\left[\Psi(s_1,\sigma_1;\ldots;\sigma_i,-s_i;\ldots;s_n,\sigma_n) + \Psi(s_1,\sigma_1;\ldots;-\sigma_i,s_i;\ldots;s_n,\sigma_n)\right] . \end{aligned} \tag{14}$$

Because $s_i, \sigma_i = \pm 1$, we have always $s_i = \pm\sigma_i$, and the last expression can thus be rewritten as

$$H_i^{\text{kin}\,1}\Psi(s_1,\sigma_1;\ldots;s_i,\sigma_i;\ldots;s_n,\sigma_n) = -t\left[\Psi(s_1,\sigma_1;\ldots;-s_i,\sigma_i;\ldots;s_n,\sigma_n) + \Psi(s_1,\sigma_1;\ldots;s_i,-\sigma_i;\ldots;s_n,\sigma_n)\right] . \tag{15}$$

We see that the Ising variables s_i, σ_i are decoupled both in H_i^4 and in $H_i^{\text{kin}\,1}$, and the latter term corresponds to the well-known transverse field. The quantum four-state clock model is thus equivalent to two *decoupled* Ising models in a transverse field equal to the original hopping parameter t, and with a new coupling constant $J/2$.

The Ising model in a transverse field was intensively studied in the 1970s. An exact solution for 1D case can be found in Ref. 25. Discussions of higher dimensionalities are given in several places.[28–30] A quantum Monte Carlo (QMC) renormalization group study of 1D and 2D cases is available in Ref. 31. In 2D at $T = 0$, there is a continuous quantum phase transition at $t/J \simeq 3.04$ between a ferroelectric state and a QPE state. The critical point extends into a line at finite temperature, where a characteristic pattern of quantum-classical crossover is realized.[32] Using the above mapping then results in a limiting value of $J_q^0/t \simeq 0.66$ for our model.

We shall come back to the simple quantum four-state clock model again in this paper, in Sec. VI, where we use this model as a test case for our path integral Monte Carlo algorithm.

IV. CONSTRAINED QUANTUM FOUR-STATE CLOCK MODEL

In this section we shall consider the constrained model, defined by the Hamiltonian

$$H^{\text{tot}} = H^4 + H^{\text{kin}\,1} + H^{\text{constr}} . \tag{16}$$

First of all we notice that the constraint eliminates a very large number of configurations. To get an insight, let us consider a 1D case for a moment, and for the sake of simplicity let us force the constraint on each other link only (Fig. 2). Clearly, the number of allowed configurations in this simplified case represents an upper limit to the number of allowed configurations in the actual 2D case.

Let us denote the total number of configurations in the chain of $2N$ sites as $b(N)$, and that of forbidden configurations as $a(N)$. Adding two new sites to the chain (increasing N by 1) amounts to increasing $b(N)$ by a factor of 4^2. The sequence $b(N)$ is therefore defined by the relation $b(N+1) = 16\,b(N)$, plus the boundary condition $b(1) = 16$, which yields $b(N) = 16^N$.

An analogous recursion formula can be found expressing the number of forbidden configurations $a(N+1)$ in the chain of $2(N+1)$ sites through the number $a(N)$ in the

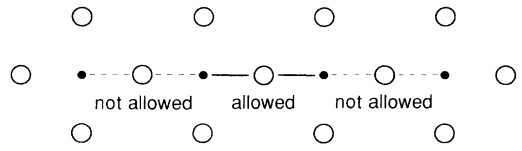

FIG. 2. 1D model chain of cages with constraint on each other link.

chain of $2N$ sites. To do so, we notice that a configuration of the chain of $2(N+1)$ sites is forbidden when *either* the two additional sites are in their single forbidden configuration while the original $2N$ sites are in any of the total of their $b(N)$ configurations, *or* when the additional sites are in any of their 15 allowed configurations, but the original $2N$ sites are in one of their $a(N)$ forbidden configurations. The sequence $a(N)$ therefore satisfies the recursion formula $a(N+1) = 15a(N) + b(N)$ with boundary condition $a(1) = 1$. The explicit expression for $a(N)$ is thus $a(N) = 16^{N-1} + 15 \times 16^{N-2} + \cdots + 15^{N-2} \times 16 + 15^{N-1}$.

We are interested in the ratio $\frac{a(N)}{b(N)}$ and its limit as $N \to \infty$. Using the above expressions for $a(N)$ and $b(N)$ we find that $\frac{a(N)}{b(N)} = 1 - (\frac{15}{16})^N \to 1$, as $N \to \infty$, which means that in the thermodynamic limit *the constraint eliminates "all" the configurations*, except for a set of zero measure. More precisely, the ratio of dimensionality of the constrained Hilbert space to that of the unconstrained one goes to zero in the thermodynamic limit, which means that the constrained space is *orthogonal* to the original one.[33]

To start with, we shall investigate the properties of the constrained quantum four-state clock model for the specially simple case $J = 0$. In this limit, it is very easily checked that the ground state of the unconstrained system ($U = 0$) is nondegenerate, and is described by a wave function Ψ_g^0, which is just a constant. This state can be seen as the product of N separate identical wave functions for each cell, each corresponding to the $j = 0$ angular momentum state of that cell. The corresponding many-body first excited state is infinitely degenerate. If we choose to label the wave functions by a wave vector $\mathbf{k}$, we have for each $\mathbf{k}$ two independent states, described respectively by the wave functions (unnormalized)

$$\Psi_{\mathrm{exc1}}^0(\mathbf{k}, z_1, \ldots, z_n) = \sum_i e^{i\mathbf{k}\cdot\mathbf{R}_i} \mathrm{Re}\, z_i \Psi_g^0, \tag{17}$$

$$\Psi_{\mathrm{exc2}}^0(\mathbf{k}, z_1, \ldots, z_n) = \sum_i e^{i\mathbf{k}\cdot\mathbf{R}_i} \mathrm{Im}\, z_i \Psi_g^0\,, \tag{18}$$

where $\mathbf{R}_i$ is the ordinary (real) vector defining the position of site i. In the absence of the constraint, i.e., for $U = 0$, the first excited state is separated from the ground state by an energy gap $2t$ (in the rest of this section we shall always set $t = 1$).

What about the $U = \infty$ constrained model? Guided by having solved first the two-site problem, we try as an ansatz for the ground state wave function of the constrained system the following (Jastrow-like) product state:

$$\Psi_g^\infty(z_1, \ldots, z_n) = \prod_{\langle ij \rangle} (\mid z_i - r_{ij} \mid + \mid z_j + r_{ij} \mid)\,, \tag{19}$$

which contains no free parameters. This wave function vanishes identically when the bond on site i points towards site j *and* the bond on site j points towards site i. It is quite close to an exact solution for two sites only.

We shall also assume that the first excited state of the constrained system corresponds to $\mathbf{k} = 0$ and can be obtained as the analytic continuation of the corresponding state (17) from $U = 0$ to $U = \infty$. In this way we arrive at the wave function

$$\Psi_{\mathrm{exc1}}^\infty(\mathbf{k} = 0, z_1, \ldots, z_n) = \sum_i \mathrm{Re}\, z_i \Psi_g^\infty(z_1, \ldots, z_n)\,, \tag{20}$$

and analogously for the degenerate state $\Psi_{\mathrm{exc2}}^\infty$.

To test these guessed wave functions in the real 2D case, defined by the constrained Hamiltonian (16), we have performed a diagonalization for a 2×2 and a 3×3 system with periodic boundary conditions (Lanczos diagonalization). In Table I we show the overlap of trial states (19) and (20) with the exact wave functions, and compare the corresponding ground state and excitation energies. It turns out that (19) is an excellent approximation for the ground state of these small systems, and the same is true for the excited state ansatz (20). We feel therefore encouraged to adopt (19) and (20) as reasonable approximations for larger systems, where diagonalization is impossible.

In order to extract properties, such as average energy and ground state correlations, and the excitation gap of the system in the thermodynamic limit, we still need to

TABLE I. Properties of the ansatz wave functions (19), (20) as compared to exact wave functions for small systems, 2×2 and 3×3.

	2×2	3×3
E_g^{exact}	-5.831	-12.607
$\langle \Psi_g^\infty \mid H \mid \Psi_g^\infty \rangle$	-5.827	-12.508
$\langle \Phi_g^{\mathrm{exact}} \mid \Psi_g^\infty \rangle$	0.9997	0.986
$E_{\mathrm{exc}}^{\mathrm{exact}}$	-4.903	-11.906
$\langle \Psi_{\mathrm{exc1}}^\infty \mid H \mid \Psi_{\mathrm{exc1}}^\infty \rangle$	-4.866	-11.818
$\mid \langle \Phi_{\mathrm{exc}}^{\mathrm{exact}} \mid \Psi_{\mathrm{exc1}}^\infty \rangle \mid^2 + \mid \langle \Phi_{\mathrm{exc}}^{\mathrm{exact}} \mid \Psi_{\mathrm{exc2}}^\infty \rangle \mid^2$	-	0.971
$\langle \Phi_{\mathrm{exc1}}^{\mathrm{exact}} \mid \Psi_{\mathrm{exc1}}^\infty \rangle$	0.995	-

calculate averages on states (19) and (20). For a 3×3 system with periodic boundary conditions the constrained Hilbert space contains 57 376 states; however, for a 4×4 system this number is 284 465 424, and regular sums over the configurations are no longer feasible in a straightforward way. We have thus adopted a Monte Carlo sampling procedure for this purpose. Energy, for example, is evaluated as the average local energy $E_{\rm loc}(j)$,

$$E = \frac{\langle\Psi \mid H^{\rm kin\,1} \mid \Psi\rangle}{\langle\Psi \mid \Psi\rangle} = (\langle\Psi \mid \Psi\rangle)^{-1} \sum_j \mid \Psi(j) \mid^2 \frac{H^{\rm kin\,1}\Psi(j)}{\Psi(j)} = \left(\sum_j \mid \Psi(j) \mid^2\right)^{-1} \sum_j \mid \Psi(j) \mid^2 E_{\rm loc}(j)\,, \quad (21)$$

where j labels the configurations of the whole system (and we recall that we are still discussing the case $J = 0$).

We have calculated the average energies of states (19) and (20) for several system sizes up to 30×30. The relevant information obtained from this calculation is summarized in Figs. 3 and 4. In Fig. 3 we have plotted the energy gap ΔE versus system size L, which shows that the gap tends to a value close to $\frac{1}{2}$ as $L \to \infty$ and $U \to \infty$. Comparison with the unconstrained gap value $\Delta E = 2$ (for $U = J = 0$) shows that the constraint acts to increase the tendency to ferroelectricity quite strongly.

In Fig. 4 we show a plot of ground state energy per site as a function of L, and we see that the finite-size energy corrections scale exponentially with L. This agrees well with the existence of an excitation gap. The correlation length obtained from energy corrections is $\xi \simeq 0.72$, which agrees with absence of long-range order. To clarify this point, we calculated the correlation function $\langle z_i^* z_j\rangle$ in the ground state, and found that it falls off very quickly with distance. It was not possible to investigate accurately its large distance behavior, because the corresponding values were close to zero and suffered from large statistical error. For illustration, we present in Table II some data for the 10×10 system. This behavior of the correlation function supports the conjecture drawn from finite-size scaling of the ground state energy, and

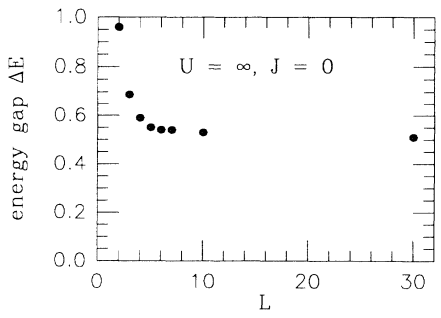

FIG. 3. Size dependence of the variational energy gap ΔE for $J = 0$, $U = \infty$, between ground state (19) and excited state (20).

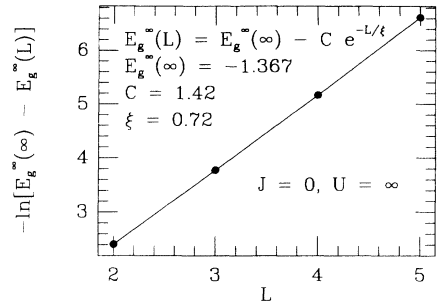

FIG. 4. Finite-size scaling to the variational ground state energy $E_g^\infty(L)$ for $J = 0$, $U = \infty$. Note the clear exponential behavior, compatible with a gap, as in the Fig. 3.

leaves us with very little doubt that ansatz (19) for the $J = 0, U = \infty$ state is disordered.

Unfortunately, we have not been able to construct simple variational states, yielding a similar semianalytical understanding of the constrained quantum model for a general $J \neq 0$. A simple correlated Jastrow form would necessarily overemphasize the disordered phase, similarly to the case of liquid ^{4}He, where such simple wave functions strongly overestimate the crystallization pressure. Zero temperature ordering in d dimensions in presence of quantum fluctuations actually corresponds to a classical ordering in $d + 1$ dimensions in presence of thermal fluctuations. In a 3D system, long-range order sets on at *much lower value* of short-range order than in a 2D system. A possible way out might perhaps be a wave function analogous to shadow wave functions, commonly used for ^{4}He, which take better account of many-body correlations.

In order to get at least a crude prediction for the critical value J_q/t, we have done a slave-boson mean-field calculation, which is presented in the Appendix. According to this approximate theory, there is already for $J = 0, U = \infty$, a ferroelectric state which is degenerate in energy with the paraelectric one. This would suggest a critical value $J_q/t = 0$, which is not compatible with the above result obtained from the ansatz (19). In the following sections, we shall resolve this issue by means of a numerical path-integral Monte Carlo simulation. Before doing so, we present a simple argument which suggests that J_q/t should be finite also for the constrained 2D quantum four-state clock model. As can be easily shown, the dielectric susceptibility of a single four-state rotor at zero temperature is $\chi_0 = 1/2t = 1/\Delta E$, where ΔE is the energy gap. Since each rotor has four nearest neighbors, a simple standard mean-field scheme would suggest a para-ferro transition at $4\,\chi_0\,J_q = 1$. For a simple, unconstrained model this yields a critical value of $J_q^0/t = 1/2$, to be compared with the true value 0.66. Since in the constrained case the gap is smaller roughly by a factor of 4, the predicted critical value correspondingly becomes equal to $J_q/t = 1/8 = 0.125$. As we shall see later, this value is again reasonably accurate. The basic fact that J_q/t remains finite, in spite of the constraint, will be confirmed. Hence, exact degeneracy of the ferro and para state at $J = 0$ is an artifact of the slave boson approximation.

TABLE II. Correlation function $\langle z_i^* z_j \rangle$ of the ground state ansatz wave function (19) for a 10×10 system.

i	j	$\langle z_i^* z_j \rangle$
(1,1)	(1,2)	0.149
(1,1)	(1,3)	$3. \times 10^{-2}$
(1,1)	(1,4)	$(7.2 \pm 2.5) \times 10^{-3}$

V. QUANTUM MONTE CARLO TECHNIQUE

In this section we shall describe the path-integral quantum Monte Carlo algorithm implemented for the simulation of the constrained model (16). The first problem to be resolved is the choice of a convenient decomposition of the Hamiltonian in order to apply the Trotter formula.

Since we are interested in the $U \to \infty$ limit of the Hamiltonian (16), we need to be especially careful. Splitting naively $H^{\rm tot}$ into the sum of a kinetic and potential energy yields in the limit $U \to \infty$ a very poor convergence of the Trotter expansion, because the commutator of the kinetic energy operator and the unbounded potential energy operator is also unbounded. The error decreases slowly, as $1/m$, with the number of Trotter slices m, analogously to that of Ref. 34. In order to avoid this problem, we have to get rid of the unbounded term in the Hamiltonian. For this purpose it is useful to introduce a projector P,

$$P = \prod_{\langle ij \rangle} (1 - P'_{ij}) = \prod_{\langle ij \rangle} P_{ij} \,, \tag{22}$$

which projects out the forbidden states. The partition function of (16) in the limit $U \to \infty$ then can be written as

$$Z = \mathrm{Tr}\, P e^{-\beta PHP} \,, \tag{23}$$

where we again denote by H the unconstrained Hamiltonian (11),

$$H = H^4 + H^{\rm kin\,1} = \sum_i (H_i^4 + H_i^{\rm kin\,1}) = \sum_i H_i \,. \tag{24}$$

It is now convenient to use both *row and column* indices i, j to label the sites of the square lattice, and write the Hamiltonian as

$$\begin{aligned} H = \sum_{ij} H_{ij} &= \sum_{(i+j)\ \text{odd}} H_{ij} + \sum_{(i+j)\ \text{even}} H_{ij} \\ &= \sum_{(i+j)\ \text{odd}} A_{ij} + \sum_{(i+j)\ \text{even}} B_{ij} \,, \end{aligned} \tag{25}$$

where A_{ij} is just a renaming of H_{ij} for the $(i+j)$ odd sublattice, and B_{ij} that for the even sublattice. Since both H and P contain only nearest-neighbor interactions, we have

$$\Big[PA_{ij}P, PA_{i'j'}P\Big] = \Big[PB_{ij}P, PB_{i'j'}P\Big] = 0 \,, \tag{26}$$

which provides us with a useful decomposition of the Hamiltonian for application of the Trotter formula. The whole lattice is decomposed into two interpenetrating sublattices A and B, each sublattice consisting of sites which do not interact with each other and are subject to an external field determined by the configuration of the other sublattice. This scheme is actually a version of the well-known checkerboard decomposition.[15]

To proceed, we write the partition function of the system as

$$Z = \mathrm{Tr}\, P\, e^{-\beta PHP} = \sum_{\{z_{ij}\}} \langle z_{ij}| P \left[e^{-\frac{\beta}{m}\left(\sum_{ij} PA_{ij}P + \sum_{ij} PB_{ij}P\right)} \right]^m |z_{ij}\rangle \,, \tag{27}$$

where m is an integer, and $|z_{ij}\rangle$ are eigenstates of the complex coordinates z_{ij} (1).

We define the mth approximant to the partition function by

$$\begin{aligned} Z_m &= \sum_{\{z_{ij}\}} \langle z_{ij}| P \left[e^{-\frac{\beta}{m}\sum_{ij} PA_{ij}P} e^{-\frac{\beta}{m}\sum_{ij} PB_{ij}P} \right]^m |z_{ij}\rangle \\ &= \sum_{\{z_{ij}^1\}} \cdots \sum_{\{z_{ij}^{2m}\}} \langle z_{ij}^1| P e^{-\frac{\beta}{m}\sum_{ij} PA_{ij}P} |z_{ij}^2\rangle \langle z_{ij}^2| P e^{-\frac{\beta}{m}\sum_{ij} PB_{ij}P} |z_{ij}^3\rangle \\ &\quad \times \cdots \langle z_{ij}^{2m-1}| P e^{-\frac{\beta}{m}\sum_{ij} PA_{ij}P} |z_{ij}^{2m}\rangle \langle z_{ij}^{2m}| P e^{-\frac{\beta}{m}\sum_{ij} PB_{ij}P} |z_{ij}^1\rangle \,, \end{aligned} \tag{28}$$

where we have inserted a complete set of intermediate states between each two exponentials. Due to (26), the matrix elements between the intermediate states in the last expression factorize, and we get

$$Z_m = \sum_{\{z_{ij}^1\}} \cdots \sum_{\{z_{ij}^{2m}\}} \prod_{k,(i+j)\,\text{odd}} \langle z_{i+1,j}^k, z_{i,j+1}^k, z_{i-1,j}^k, z_{i,j-1}^k, z_{i,j}^k | P e^{-\frac{\beta}{m} P A_{ij} P} | z_{i+1,j}^{k+1}, z_{i,j+1}^{k+1}, z_{i-1,j}^{k+1}, z_{i,j-1}^{k+1}, z_{i,j}^{k+1} \rangle$$
$$\times \prod_{k,(i+j)\,\text{even}} \langle z_{i+1,j}^k, z_{i,j+1}^k, z_{i-1,j}^k, z_{i,j-1}^k, z_{i,j}^k | P e^{-\frac{\beta}{m} P B_{ij} P} | z_{i+1,j}^{k+1}, z_{i,j+1}^{k+1}, z_{i-1,j}^{k+1}, z_{i,j-1}^{k+1}, z_{i,j}^{k+1} \rangle , \tag{29}$$

where $|z_{i+1,j}^k, z_{i,j+1}^k, z_{i-1,j}^k, z_{i,j-1}^k, z_{i,j}^k\rangle = |z_{i+1,j}^k\rangle |z_{i,j+1}^k\rangle |z_{i-1,j}^k\rangle |z_{i,j-1}^k\rangle |z_{i,j}^k\rangle$. It is easily seen that the matrix elements in the last equation are *diagonal* in the quantum numbers $z_{i+1,j}^k, z_{i,j+1}^k, z_{i-1,j}^k, z_{i,j-1}^k$, and can therefore be written as

$$\langle z_{i+1,j}^k, z_{i,j+1}^k, z_{i-1,j}^k, z_{i,j-1}^k, z_{i,j}^k | P e^{-\frac{\beta}{m} P H_{ij} P} | z_{i+1,j}^k, z_{i,j+1}^k, z_{i-1,j}^k, z_{i,j-1}^k, z_{i,j}^{k+1} \rangle$$
$$= C(z_{i+1,j}^k, z_{i,j+1}^k, z_{i-1,j}^k, z_{i,j-1}^k, z_{i,j}^k, z_{i,j}^{k+1}) . \tag{30}$$

This diagonality imposes a conservation rule on the (2+1)-dimensional classical system on which our 2D quantum system maps. The mapping now follows from

$$Z_m = \sum_{\{z_{ij}^1\}} \cdots \sum_{\{z_{ij}^{2m}\}} \prod_{k,(i+j)\,\text{odd}} C(z_{i+1,j}^k, z_{i,j+1}^k, z_{i-1,j}^k, z_{i,j-1}^k, z_{i,j}^k, z_{i,j}^{k+1})$$
$$\times \prod_{k,(i+j)\,\text{even}} C(z_{i+1,j}^k, z_{i,j+1}^k, z_{i-1,j}^k, z_{i,j-1}^k, z_{i,j}^k, z_{i,j}^{k+1}) , \tag{31}$$

and each term in the above product can be interpreted as a Boltzmann factor of a parallelepiped with corners in the points $(i+1,j,k)$, $(i,j+1,k)$, $(i-1,j,k)$, $(i,j-1,k)$, $(i+1,j,k+1)$, $(i,j+1,k+1)$, $(i-1,j,k+1)$, $(i,j-1,k+1)$ of the (2+1)-dimensional lattice (Fig. 5). There is a four-state clock rotor in each of its corner points, as well as in the centers (i,j,k), $(i,j,k+1)$ of both its horizontal faces. The corresponding classical system can thus be seen as a (2+1)-dimensional lattice of such parallelepipeds. The conservation rule restricts *both rotors in the upper and the lower corners of the vertical edges of each parallelepiped to be in the same state.* The Boltzmann weight (30) of each parallelepiped then depends on the state of all four rotors in its vertical edges, as well as on the state of both rotors in the centers of its horizontal faces. The mutual state of these latter rotors, sitting in the centers of the horizontal faces, *is not restricted* in any way (Fig. 5).

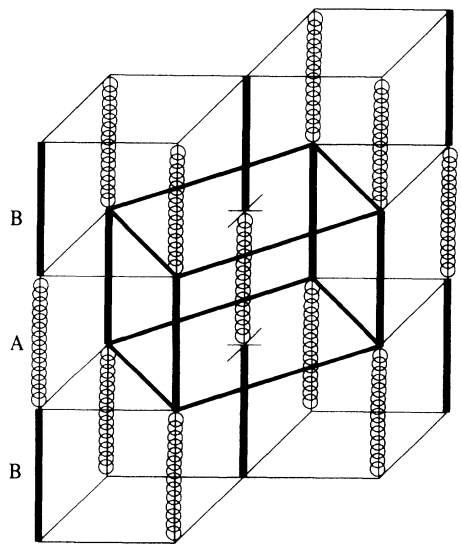

FIG. 5. The (2+1)-dimensional classical system. The imaginary time (Trotter) direction is vertical. Vertical dark lines connect sites, which must be flipped together; springs connect independent sites.

The calculation of the matrix elements $C(z_{i+1,j}^k, z_{i,j+1}^k, z_{i-1,j}^k, z_{i,j-1}^k, z_{i,j}^k, z_{i,j}^{k+1})$ is straightforward. It requires just diagonalization of the 4×4 on-site problem of a four-state clock rotor $H_i^{\text{kin}\,1}$ in an external field, represented by H_i^4 and the projector P. In our simulation we performed this diagonalization numerically. All the matrix elements turned out to be non-negative, and therefore no sign problem was present.[35]

We proceed to identify the estimators for the thermodynamic quantities. For convenience we write the partition function approximant Z_m symbolically as

$$Z_m = \sum_{\{z_{ij}^1\}} \cdots \sum_{\{z_{ij}^{2m}\}} \prod_{k,i,j}{}' C_{kij} , \tag{32}$$

where $\prod'_{k,i,j}$ means a product over such k,i,j that k and $(i+j)$ have the same parity. The internal energy per site of the system then reads

$$E_m = -\frac{1}{N}\frac{1}{Z_m}\frac{\partial Z_m}{\partial \beta} = \langle E_{\text{est}} \rangle , \tag{33}$$

where

$$E_{\text{est}} = -\frac{1}{N}\sum_{k,i,j}{}' \frac{1}{C_{kij}}\frac{\partial C_{kij}}{\partial \beta} \tag{34}$$

is the corresponding estimator. For the specific heat per site c_v we obtain

$$c_{vm} = -\frac{1}{N}\beta^2 \frac{\partial E_m}{\partial \beta}$$
$$= \frac{1}{N}\beta^2 \left\{ \langle E_{\rm est}^2 \rangle - \langle E_{\rm est} \rangle^2 + \left\langle {\sum_{k,i,j}}' \left[\frac{1}{C_{kij}} \frac{\partial^2 C_{kij}}{\partial \beta^2} - \left(\frac{1}{C_{kij}} \frac{\partial C_{kij}}{\partial \beta} \right)^2 \right] \right\rangle \right\} , \tag{35}$$

and we see that it is not just equal to the fluctuation of the internal energy, as in the classical case. The Hamiltonian of our effective classical system is itself temperature dependent.

In order to calculate the order parameter, which in our case is the polarization of the system, and the corresponding susceptibility, we have to consider an external field F applied on the system. If we choose this to point, e.g., along the x axis, the matrix elements $C(z^k_{i+1,j}, z^k_{i,j+1}, z^k_{i-1,j}, z^k_{i,j-1}, z^k_{i,j}, z^{k+1}_{i,j})$ in (31) are replaced by

$$C(z^k_{i+1,j}, z^k_{i,j+1}, z^k_{i-1,j}, z^k_{i,j-1}, z^k_{i,j}, z^{k+1}_{i,j}) \to C(z^k_{i+1,j}, z^k_{i,j+1}, z^k_{i-1,j}, z^k_{i,j-1}, z^k_{i,j}, z^{k+1}_{i,j}) \exp\left(\frac{\beta}{m} F \,\mathrm{Re}\, z^k_{i,j} \right) , \tag{36}$$

and we obtain, for the equilibrium polarization per site P_{xm},

$$P_{xm} = \frac{1}{\beta N Z_m} \frac{\partial Z_m}{\partial F} = \langle P_{xm\,\rm est} \rangle , \tag{37}$$

where

$$P_{xm\,\rm est} = \frac{1}{Nm} {\sum_{k,i,j}}' \mathrm{Re}\, z^k_{i,j} . \tag{38}$$

The static dielectric susceptibility $\chi_{xx\,m}$ then turns out to be

$$\chi_{xx\,m} = \frac{\partial P_{xm}}{\partial F} = \beta N \left[\langle P^2_{xm\,\rm est} \rangle - \langle P_{xm\,\rm est} \rangle^2 \right] . \tag{39}$$

The last two quantities are suitable to study the system either in the paraelectric phase, where $\langle P_{xm\,\rm est} \rangle = 0$, or in the ferroelectric phase not very close to the transition, when the order parameter does not undergo the finite-size flipping among the four possible orientations, and $\langle P_{xm\,\rm est} \rangle$ remains a well-defined quantity during the simulation time. For the behavior of the system right across the phase transition, it is convenient to monitor the modulus rather than the components of the order parameter. We have

$$P_m = \langle P_{m\,\rm est} \rangle = \langle \sqrt{P^2_{xm\,\rm est} + P^2_{ym\,\rm est}} \rangle , \tag{40}$$

and the corresponding susceptibility is given by

$$\chi_m = \beta N \left[\langle P^2_{m\,\rm est} \rangle - \langle P_{m\,\rm est} \rangle^2 \right] . \tag{41}$$

Finally, we have sampled a "short-range order parameter" $\langle \cos(\phi_i - \phi_j) \rangle$ (we again denote a site of the 2D lattice by just one index i), where i, j are nearest neighbors. This can be calculated as

$$\langle \cos(\phi_i - \phi_j) \rangle$$
$$= \frac{1}{2Nm} \left\langle {\sum_{k,i}}' \left[\mathrm{Re}(z_i^{k*} z^k_{i+\mathbf{x}}) + \mathrm{Re}(z_i^{k*} z^k_{i+\mathbf{y}}) \right] \right\rangle . \tag{42}$$

Our (2+1)-dimensional classical system is simulated in a standard way using the Metropolis algorithm. The trace operation requires periodic boundary conditions along the imaginary time direction. We have used periodic boundary conditions for both space directions as well. In order to satisfy the conservation rule, we must always move the pairs of rotors on both sides of the vertical edges of the parallelepipeds simultaneously. It is therefore convenient to consider the vertical edges as being a kind of "rigid rods" and take these as new variables, which now can be moved independently (Fig. 5). One randomly chosen rod was moved at a time, without any kind of collective moves. Unlike in simulation of the classical four-state clock model,[36] we did not restrict the flips of the rods and allowed these to flip from the present position to each of the remaining three.

We carried out almost all calculations by fixing the value of the ferroelectric coupling J and of the number of Trotter slices m, and then running a series of simulations for different temperatures. The final configuration of a simulation at a given temperature was used as the initial configuration for a run at the next higher temperature, always heating the system. As the initial configuration at the lowest temperature, we always took the ferroelectric state, completely ordered both in space and in the imaginary time directions. (The only exception is the data shown on Fig. 12, where the corresponding runs were carried out at constant temperature, decreasing the value of J.) We typically used 1–2×10^4 MC steps/site to equilibrate the system and 2–4×10^5 MC steps/site for calculating averages. The CPU time needed to perform 1 MC step/site was about 14 μs using an HP720 RISC machine.

In order to estimate the statistical accuracy of our results we measured the MC correlation time of the chain of values generated for various quantities in course of the simulation. We did this by using the standard method of dividing the chain in blocks of variable size described in Refs. 37, 38.

To end this section, we would like to comment briefly on the convergence of the averaged quantities as a function of the number of Trotter slices m. It is well known[15] that the error in the average value of an operator due to the Trotter decomposition is an even function of m and therefore the results of a QMC simulation can, in principle, be extrapolated to $m \to \infty$ in the form

$$A_m = A_\infty + \frac{a}{m^2} + \frac{b}{m^4} + \cdots . \tag{43}$$

This kind of extrapolation, to be meaningful, would require very high accuracy simulation for at least two values of m (to determine a), or three values of m (to determine b), etc. For most data presented in this paper (the only exception being the dielectric susceptibility curve of the unconstrained model for $J = 0.5$) such a procedure was not performed. Except at the lowest temperatures, it was generally sufficient to inspect the data for $m = 5, m = 10$ or $m = 10, m = 20$ (at the lowest temperatures investigated, we have sometimes used also $m = 40$) to see that further increasing of m would not change the value of the quantity under consideration within our statistical accuracy. We shall come back to this point in more detail when presenting the actual results of the simulation.

VI. TEST OF THE PIMC SCHEME: THE UNCONSTRAINED QUANTUM FOUR-STATE CLOCK MODEL

In order to test the QMC scheme described in the last section, we chose to perform a simulation of a limited extent for the simple unconstrained model, which is equivalent to the quantum Ising model, as discussed in Sec. III. Here we describe some of these results, since they will also be of interest for comparison with those obtained for the constrained model in the next section.

As an initial test, we did a numerical diagonalization of a 2×2 system with $J = 0.5$, and compared the exact canonical results for internal energy and specific heat with those of the PIMC simulation. In order to obtain a good statistical accuracy, we used 1×10^6 MC steps/site for the simulation, and found excellent agreement (Fig. 6).

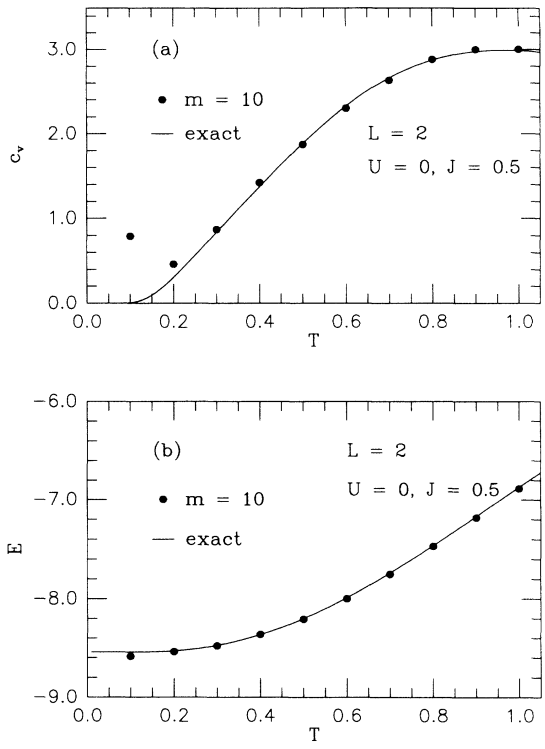

FIG. 6. Test of the PIMC method: specific heat c_v (a) and internal energy E (b) for a 2×2 unconstrained system with $J = 0.5$, as obtained from the simulation, to be compared with the exact result obtained from the diagonalization.

Next, we carried out simulations for three different values of $J = 1.0, 0.75, 0.5$ ($t = 1$). The first value $J = 1.0$ was found to correspond to the nearly classical regime of the system, which is not of our interest, and we shall not describe the results for this case in detail. Since in Sec. III we found that $J_q^0/t \simeq 0.66$, each of the latter two values of J is expected to correspond to a different regime of the system. The results can be described as follows.

For $J = 0.75$, the simulation was done for three different lattice sizes $L = 6, 10, 20$ and the corresponding results are shown in Fig. 7. The zero temperature value of $|P|$ is about 0.65, which reveals the effect of quantum fluctuations. The ferroelectric-paraelectric transition is seen as a drop of $|P|$ and as a sharp critical peak of the dielectric susceptibility curve near a $T_c \sim 0.5$.

In order to extrapolate the infinite-size critical temperature, we have analyzed our data using the phenomenological renormalization method,[13] which treats properly the large finite-size corrections. The analysis of the susceptibility (Fig. 8) agrees with a critical temperature of $T_c \simeq 0.5$ and a ratio of critical exponents $\frac{\gamma}{\nu}$ close to the 2D Ising value of $\frac{7}{4}$. Since the classical transition temperature for $J = 0.75$ is $T_c = 0.851$, the effect of quantum fluctuations has been to reduce T_c quite considerably. An interesting feature is the behavior of the specific heat. It has a rather flat maximum at temperatures almost twice as high as the transition temperature, with no strong evidence of critical behavior at T_c itself, for the system sizes we studied. This is again a sign that the system is in a quantum regime, and one would have to go to larger sizes to observe the expected crossover[32] from quantum to classical critical behavior, sufficiently close to T_c.

For $J = 0.5$, we ran the simulation for only one lattice size, namely, $L = 10$. The results are in Figs. 9 and 10. Ferroelectricity seems altogether absent, all the way down to $T = 0$ (Fig. 9). To clarify further this case, we also performed an extrapolation of the dielectric susceptibility to $m \to \infty$ and found it to saturate at low temperatures. This means that the paraelectric state persists down to the lowest temperatures and we therefore conclude that for this value of J the system is at low temperatures in the quantum paraelectric regime.

Apart from the usual long-range order parameter $|P|$, we can also demonstrate the temperature dependence of the nearest-neighbor "short-range order parameter" $\langle \cos(\phi_i - \phi_j) \rangle$ (Fig. 10). Since the system is now paraelectric for all temperatures, $|P|$ must scale to zero with increasing system size L. Its behavior for a finite L reflects that of the correlation length ξ. The polarization $|P|$ is seen to pass through a moderate *maximum* at temperature $T^* \sim 0.6$, where the same kind of behavior is clearly visible also on the nearest-neighbor order $\langle \cos(\phi_i - \phi_j) \rangle$ curve. The correlation length ξ of a system in the quantum paraelectric regime thus has a maximum at a finite T^*. This kind of effect, in the different context of granular superconductors, was found by Fazekas

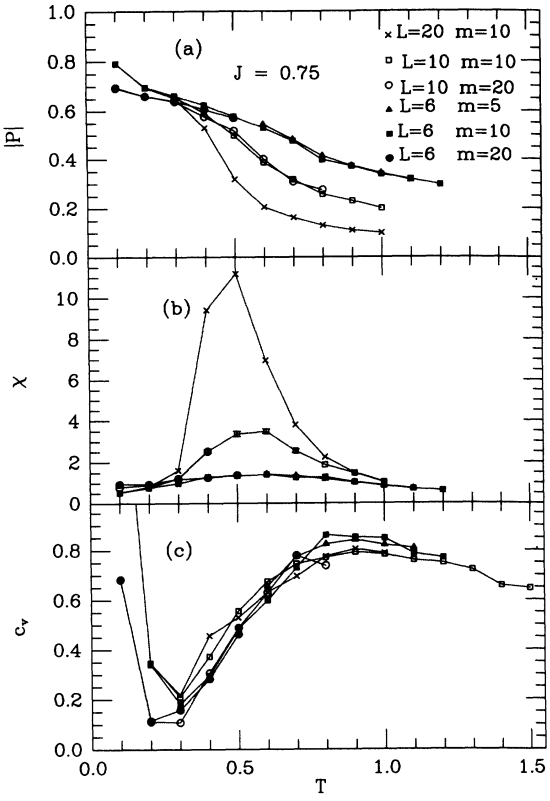

FIG. 7. Polarization $|P|$ (a), dielectric susceptibility χ (b), and specific heat c_v (c) for $J = 0.75$, $U = 0$. There is evidence of a ferro-para transition near $T_c \sim 0.5$. The singularity of c_v is severely depressed by quantum effects.

et al. in Ref. 39, where a continuous XY model was investigated. Their conclusion as to the existence of a broad maximum of short-range order at $T^* \sim J$ remains therefore valid also in the case of our discrete four-state clock model. Qualitatively, the interpretation of this effect is the following. At zero temperature, the rotors are predominantly in their totally symmetric ground state $|0\rangle + |\pi/2\rangle + |\pi\rangle + |-\pi/2\rangle$, corresponding to the angu-

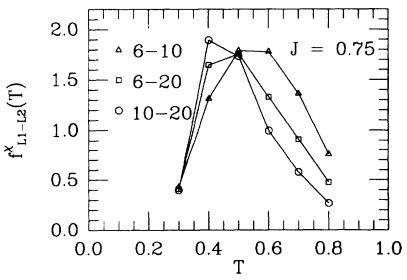

FIG. 8. Finite-size scaling determination of T_c, and $\frac{\gamma}{\nu}$ from the phenomenological renormalization method (Ref. 13). On the vertical axis is

$$f^{\chi}_{L_1 L_2}(T) = \frac{\ln[\chi(L_1,T)/\chi(L_2,T)]}{\ln(L_1/L_2)} .$$

All the curves should intersect at the point $(T_c, \frac{\gamma}{\nu})$. Our best estimate for T_c is 0.5, for $J = 0.75$, $U = 0$.

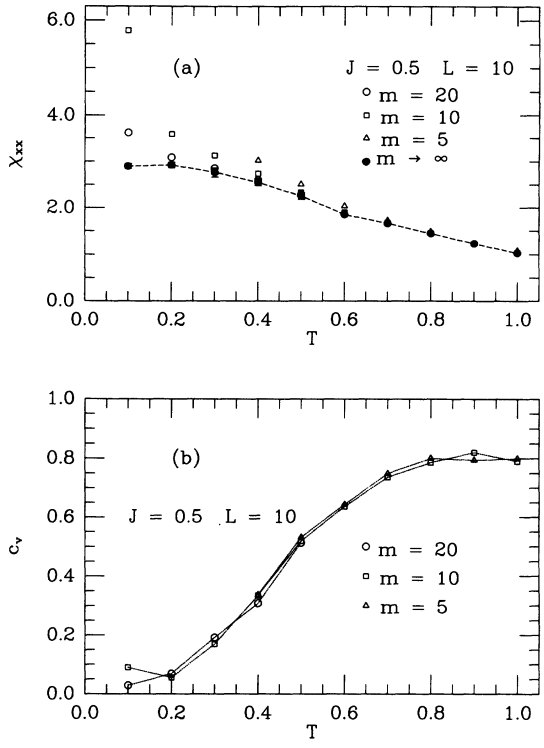

FIG. 9. Dielectric susceptibility χ_{xx} (a) and specific heat c_v (b) for $J = 0.5$, $U = 0$. Long-range ferroelectricity is absent. On cooling, the system evolves from classical paraelectric to QPE.

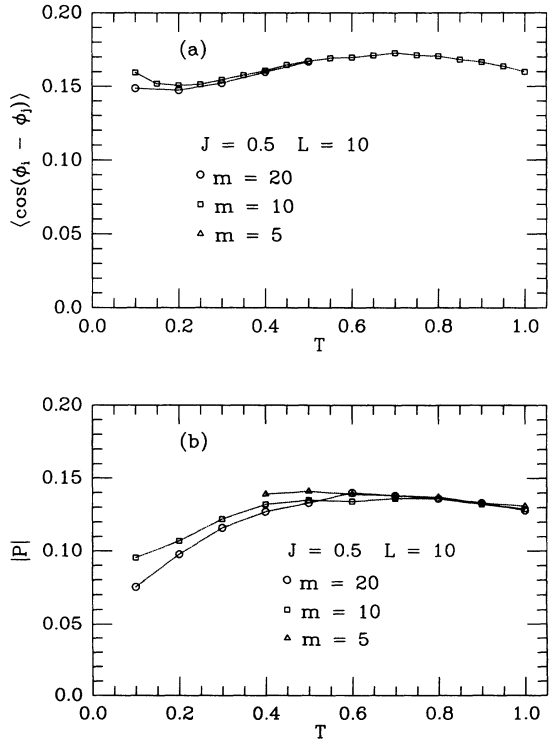

FIG. 10. Nearest-neighbor "short-range order parameter" $\langle\cos(\phi_i - \phi_j)\rangle$ (a) and polarization $|P|$ (b) for $J = 0.5$, $U = 0$. Note a mild peak of the short-range order at $T^* \sim 0.6$.

lar momentum $j = 0$, which does not possess a dipole moment. Increasing the temperature from $T = 0$, rotor states with nonzero dipole moment become thermally excited, and the system starts to develop some amount of short-range order due to the coupling J. This order reaches a maximum at finite temperature, and is then eventually disrupted by thermal fluctuations as temperature increases further.

VII. SIMULATION OF THE CONSTRAINED QUANTUM FOUR-STATE CLOCK MODEL

As a test of the code, we simulated first a 2×2 system, for $J = 0.5$, using again 1×10^6 MC steps/site, and compared the results with the exact canonical averages calculated from the numerical diagonalization. We found a very satisfactory agreement (Fig. 11). In the rest of this section, all the quantities were averaged over 4×10^5 MC steps/site, after discarding the initial 2×10^4 MC steps/site necessary for equilibration.

In Fig. 12, we plot the calculated dielectric susceptibility χ versus coupling constant J at low temperatures, $T = 0.1$ and $T = 0.2$, for system size $L = 10$. We see a sharp peak, signaling a transition, roughly at $J_c \simeq 0.17$ for $T = 0.2$ and at $J_c \simeq 0.15$ for $T = 0.1$. The limiting quantum critical value may thus be estimated to be close to $J_q/t = 0.15$, a factor of about 4 smaller than that for the unconstrained model.

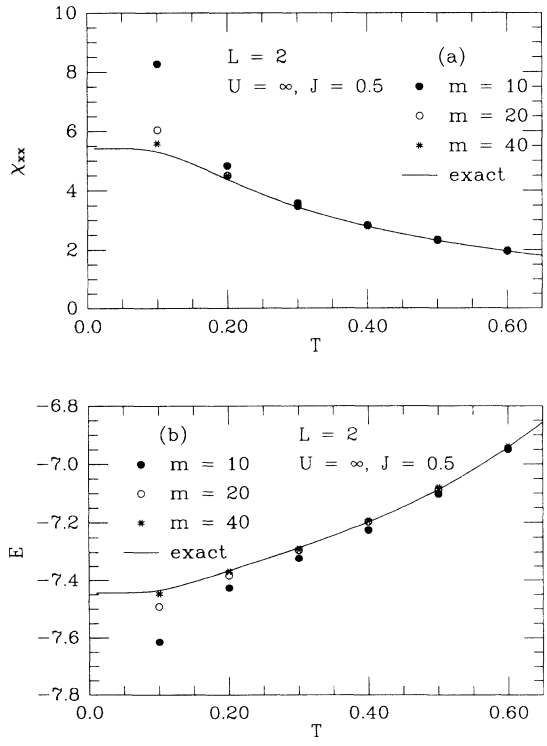

FIG. 11. Test of the PIMC method: dielectric susceptibility χ_{xx} (a) and internal energy E (b) for a 2×2 *constrained* system with $J = 0.5$, $U = \infty$, as obtained from the simulation, to be compared with the exact result obtained from the diagonalization.

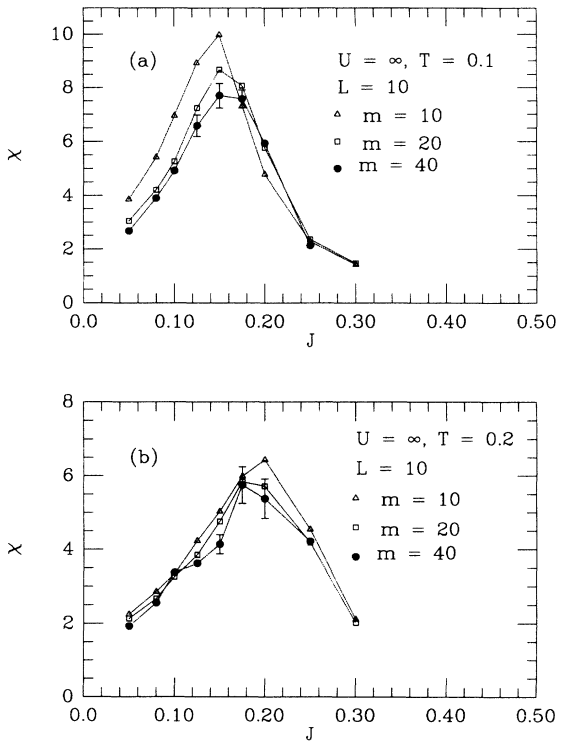

FIG. 12. Constrained model dielectric susceptibility χ as a function of coupling J, for $T = 0.1$ (a) and $T = 0.2$ (b), $U = \infty$. A ferro-para transition is evident, near $J_q/t \simeq 0.15$. Error bars represent one standard deviation from the mean.

At this point, we have to recall the limitations of the method used. It is intuitively clear that already in the classical case, the presence of the constraint acts to reduce considerably the acceptance ratio of our simple unbiased MC moves. Moreover, in the quantum case, the constraint increases the systematic error due to Trotter decomposition, and a larger number of Trotter slices is needed to approach the true quantum averages, particularly at low temperatures. This, in turn, further reduces the acceptance ratio, and problems with loss of ergodicity of the system might appear. For illustration, in the worst of the cases we studied, $T = 0.2$, $J = 0.2$, $m = 40$ (right at the phase transition), the correlation time of the chain of values generated for the polarization was $\sim$ 2000 MC steps/site, resulting in the statistical error (one standard deviation) of the dielectric susceptibility of the order of 10%. As can be seen in Fig. 12, this statistical error is already of the same order of magnitude of the Trotter error, and further increasing of m would be useless. The values of m we used were always chosen in order to achieve a compromise between the requirement of convergence and that of keeping a reasonable acceptance ratio. Typically, we used $m = 10$ Trotter slices in the temperature interval from $0.1 < T < 1$. In the low-temperature range ($T \leq 0.4$) we also used $m = 20$ and $m = 40$ Trotter slices.

These problems do not permit a simple satisfactory finite-size scaling analysis of the results.[40] Therefore, apart from the initial test, all the results in this section refer to a single system size, $L = 10$.

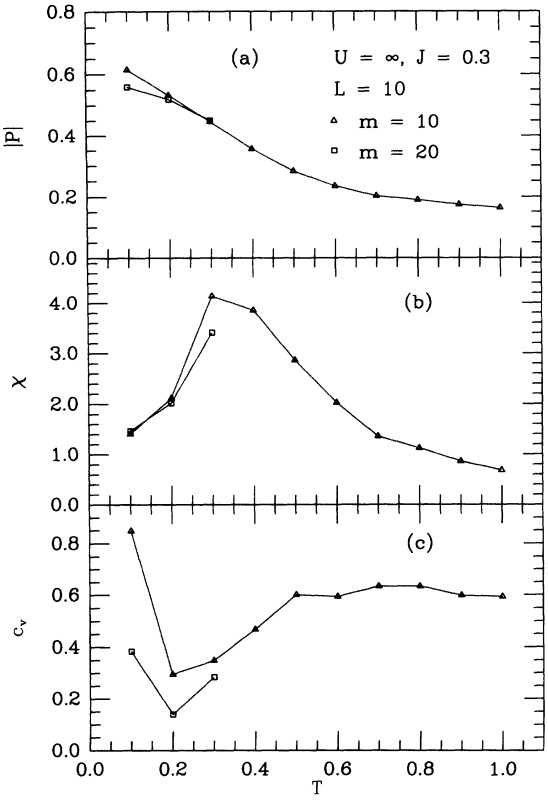

FIG. 13. Polarization $|P|$ (a), dielectric susceptibility χ (b), and specific heat c_v (c) for $J = 0.3$, $U = \infty$. There is a clear ferro-para transition near $T_c \sim 0.35$.

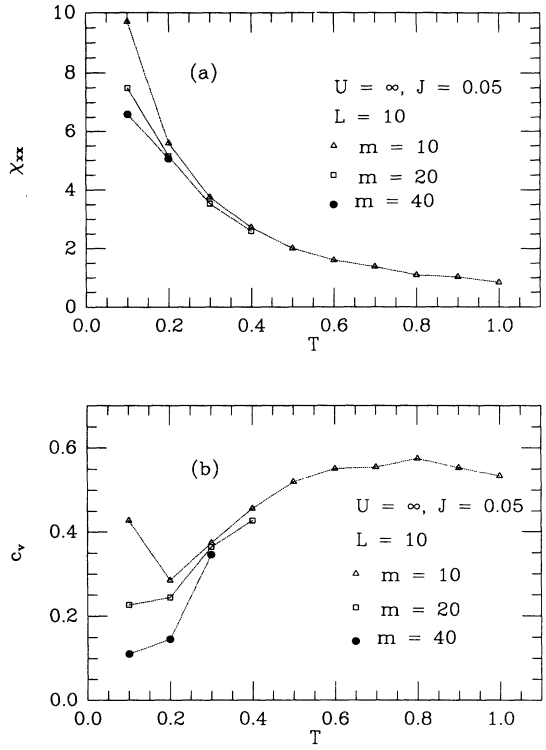

FIG. 14. Dielectric susceptibility χ_{xx} (a) and specific heat c_v (b) for $J = 0.05$, $U = \infty$. The low-temperature state is a QPE.

In Fig. 13 we plot the order parameter $|P|$, the dielectric susceptibility χ, and the specific heat c_v versus temperature for $J = 0.3$. The system is clearly ferroelectric at low temperatures. However, the saturation value of the order parameter $|P|$ is ~ 0.5, indicating a strong quantum fluctuation reduction. The susceptibility χ has a peak at $T \sim 0.35$, for this value of J. At the same temperature, however, the specific heat c_v does not show any apparent singularity for this small size. As also found in the previous section, milder specific-heat singularities are, however, quite typical for quantum transitions.[7,9]

Figures 14 and 15 present plots of the quantities χ_{xx}, c_v, and $|P|$, plus in addition the temperature dependence of the nearest-neighbor short-range order parameter $\langle\cos(\phi_i - \phi_j)\rangle$, for $J = 0.05$. For this value of the coupling constant, which is lower than J_q/t, the system should be in the quantum paraelectric regime at low T. Actually, were it not for the J dependence of χ (Fig. 12), it would be difficult to draw this conclusion just by inspection of the T dependence of χ_{xx}. In fact, even at the lowest temperatures investigated, χ_{xx} does not seem to saturate, and continues to grow with decreasing T. Further simulation for even lower temperatures in this deeply quantum regime is at the moment not feasible, with the present algorithm, for the reasons discussed above.

Similarly to the unconstrained case, the polarization $|P|$ is seen to pass through a moderate maximum at temperature $T^* \sim 0.3$, and the same behavior is now

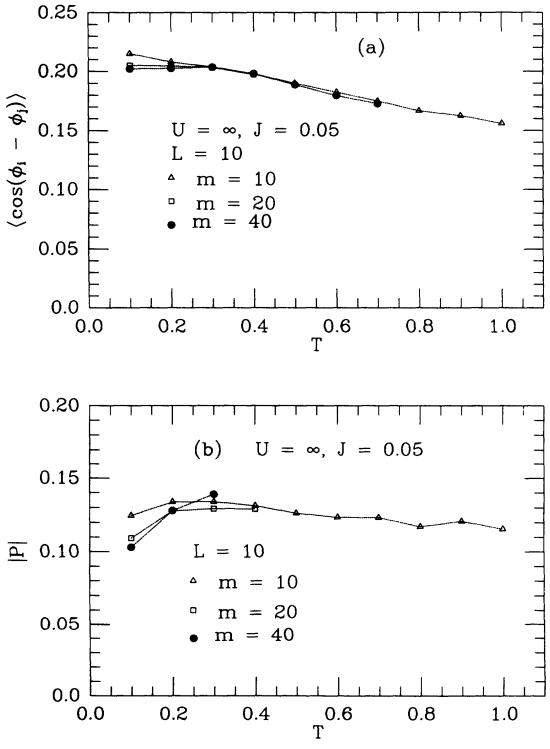

FIG. 15. Nearest-neighbor "short-range order parameter" $\langle\cos(\phi_i - \phi_j)\rangle$ (a) and polarization $|P|$ (b) for $J = 0.05$, $U = \infty$.

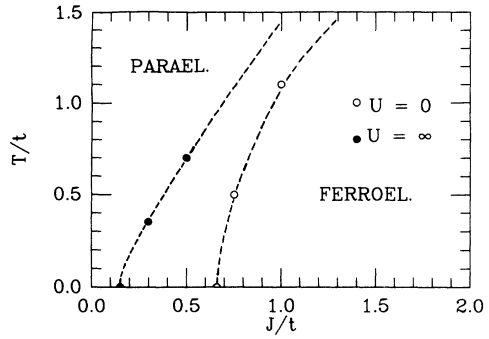

FIG. 16. Phase diagram of both unconstrained and constrained models in the $(J/t, T/t)$ plane. Note the shift of the phase boundary towards lower J/t due to the constraint.

just barely visible also on the nearest-neighbor order $\langle\cos(\phi_i - \phi_j)\rangle$. We note that the specific heat c_v is smooth, with the same broad maximum near $T \sim 0.8$ present also for the ferroelectric case $J = 0.3$. Finally, in Fig. 16, we show a sketch of phase diagrams for both the unconstrained and the constrained models, as resulting from our simulations.

The two phase diagrams are qualitatively similar. There are only two phases, the ferro and the para. The $T = 0$ QPE phase is nondegenerate, and has a gap. It will transform into a classical paraelectric with temperature, with just a smooth crossover and no phase transition.

VIII. DISCUSSION AND CONCLUSIONS

In this paper, we have studied the physics of the simplest models of QPE systems. The selection of a meaningful Hamiltonian is particularly delicate, and we have been able to make only some tentative steps towards modeling the real perovskite quantum paraelectrics $SrTiO_3$ and $KTaO_3$. Several main points have emerged in this selection process.

The first is that (unfortunately) only models capable of describing order-disorder fluctuations should be considered really adequate, since experimentally quantum perovskites appear to crossover into an order-disorder regime, *before* entering a sort of quantum central peak state at low temperatures. An alternative displacive, mean-field picture would be inadequate to describe this situation. We have therefore preferred discrete lattice models, and chosen techniques which can describe adequately fluctuations, quantum as well as classical. The basic element in our discrete lattice models is the Ti-O dipole, also called a "bond."

A second point which has emerged is that we might expect in a perovskite quantum ferroelectric at least two different quantum tunneling processes. The first is bond tunneling between the n equivalent positions inside the octahedral cage ($n = 4$ in tetragonal $SrTiO_3$, $n = 6$ in cubic $KTaO_3$). The second is bond tunneling between one cage and the next. This second process will occur whenever an oxygen which is bonded to one Ti hops to bond the other Ti, as in Fig. 1(b). In this first study, however, we have included only the first processes.

A third point is that there are two strong constraints which restrict both classical and quantum-mechanical motion, if the model is to make physical sense for real perovskites. A first constraint, probably valid at low temperatures, is that there should not be more than one bond per cell. In other words, as long as we are in the order-disorder regime, and the Ti atoms are instantaneously off center, each can engage at most one of the surrounding oxygens. The second, more interesting constraint is that two neighboring cages must not simultaneously possess bonds which point towards one another. This constraint comes from the physical impossibility of an oxygen to be engaged in two bonds simultaneously, and constitutes a kind of ice rule. The necessity of an effective ice rule in displacive perovskite ferroelectrics (or, for that matter, in cuprate high-T_c superconductors) does not seem to have been noted and made use of before, and might have far-reaching consequences.

Guided by these considerations, we have selected a short-range, 2D lattice quantum four-state clock model, as the simplest toy model of QPE perovskites. Of the ingredients mentioned above, two in particular pose some difficulty, namely, the inter-cell bond tunneling and the ice-rule constraint. Our strategy has been therefore to start off first without these two ingredients, with the simple quantum four-state clock model, and then to add the complications only gradually and successively. Since handling of bond hopping is very dependent from the presence of the ice constraint, it was necessary to include the latter first. Thus, the second discrete model considered in this paper is an ice-rule-constrained quantum four-state clock model. This still leaves out bond hopping, whose inclusion is now being actively considered, and will hopefully form the subject of the subsequent paper.

The main method adopted for the present study of the unconstrained and constrained 2D quantum four-state clock models is the path-integral Monte Carlo method (plus finite-size scaling when possible). For the unconstrained case this calculation is meant to reproduce known results, since, as we show, the model maps onto two uncoupled quantum Ising models (Ising model in a transverse field), well studied and characterized in the 1970s. The ice-rule-constrained model is instead new and nontrivial. A new simulation strategy has been devised, in order to eliminate a pathologically slow $1/m$ convergence with the number of imaginary time slices m, to recover even for the constrained model the usual, more comfortable $1/m^2$ convergence. Although we cannot push finite-size scaling to produce critical exponents for this case, we have obtained a reasonably accurate phase diagram.

There are, both in the constrained and in the unconstrained models, only two phases, the ferroelectric and the paraelectric states. However, the ice-rule constraint greatly reduces the number of excited configurations, and this in turn reinforces ferroelectricity. As a result, the extrapolated $T = 0$ critical ratio of potential to kinetic coupling parameters is $J_q/t \simeq 0.15$, a factor of about 4 smaller than that $J_q^0/t \simeq 0.66$ of the unconstrained model. The classical critical temperature will also be raised with respect to the unconstrained case, although

we did not pursue this aspect in detail. We would not be surprised if a future closer analysis of both classical and quantum critical behavior should reveal different universality classes, for the unconstrained and the ice-rule-constrained 2D clock models.

What have we learned about the nature of the QPE state in the constrained and unconstrained quantum four-state clock models? We have found that the state is fully symmetric, and has an excitation gap in both cases. However, the gap ΔE is very severely reduced by the ice-rule constraint, this reduction being about a factor of 4 at $J = 0$. As long as the ground state is nondegenerate with an excitation gap, transformation from the classical paraelectric state at high temperatures to the QPE state at low temperatures is predicted to be a smooth crossover, not a phase transition. The finding is in line with traditional views on QPE's.[3] It does not explain, however, the phase transition phenomena found by Müller *et al.*[2] in pure, tetragonal $SrTiO_3$.

To put things in the right perspective, we should however remember that the basic assumption behind our lattice model is, as stressed in Sec. II, that the dipoles, i.e., stronger Ti-O or Ta-O bonds, should exist at all temperatures. In reality, this is not the case. As mentioned in Sec. II, in $KTaO_3$ the off-center displacement of Ta ions sets up rather abruptly below $T^* \sim 40$ K, and a very similar picture is probably valid also for $SrTiO_3$. In other words, crossover from the high-temperature displacive regime, with a soft mode and no distortion, to the order-disorder regime occurs suddenly, and very close to the extrapolated displacive Curie temperature T^*. The individual dipoles of our discrete model first appear as such at this abrupt crossover temperature. The model itself, therefore, makes sense only for $T < T^*$. What should turn the expected sharp crossover into a genuine phase transition in $SrTiO_3$ remains at this stage unclear.

We are presently pursuing further the physics of these interesting phenomena, by including next the bond-hopping term, and hope to report relevant results in the near future.

ACKNOWLEDGMENTS

We wish to acknowledge fruitful discussions with, and help from, E. Courtens, A. Ferrante, M. Maglione, G. Mazzeo, K. A. Müller, and S. Sorella. Support by INFM and by the European Research Office, U.S. Army, is also acknowledged.

APPENDIX: SLAVE-BOSON MEAN-FIELD THEORY

In this appendix we present a mean-field theory for the ground state of the constrained model, at $J = 0$. From this, we also get indirectly an estimate for the critical value J_q/t. The main problem is to deal with the rigid constraint which prevents the oxygens from being doubly bonded. This feature of our model is very similar to that which applies to electrons in the infinite U Hubbard model, where the repulsion energy also eliminates double occupancy of a single site. This analogy suggests that we may try to use the method of introducing auxiliary, slave-boson fields, commonly used in the Hubbard model studies.[41]

For this purpose it is convenient to work in the occupation number representation. First of all, for each pair of nearest-neighbor sites i, j we introduce two Bose operators $b_{ij}^\dagger, b_{ji}^\dagger$. The operator $b_{ij}^\dagger$ creates a bond of the central ion on site i, pointing towards site j, and similarly $b_{ji}^\dagger$ creates a bond of the central ion on site j pointing towards site i. We notice that obviously $b_{ij}^\dagger \neq b_{ji}^\dagger$. Between the central sites i, j, there is a "bridging" oxygen ion, which can be unambiguously labeled by the pair of site labels i, j or j, i. This oxygen ion, depending on the states of central ions on sites i, j, can in fact be in four different states. In order to describe these states, we introduce new Bose operators $e_{ij}^\dagger, p_{ij,i}^\dagger, p_{ij,j}^\dagger, d_{ij}^\dagger$, with the following meaning. The oxygen is in the state $e_{ij}^\dagger |0\rangle$, if none of the central ions is bonded to it. It is in the state $p_{ij,i}^\dagger |0\rangle$, if the ion on site i is bonded to it, and analogously for $p_{ij,j}^\dagger |0\rangle$. Finally, in the state $d_{ij}^\dagger |0\rangle$, both central ions on sites i, j are bonded to it. These oxygen operators represent our auxiliary fields, or slave bosons. In our case they do correspond to real physical states of the oxygen ion, and from this point of view, they are in fact real bosons. From the way we introduced all the operators it is clear that these satisfy the following constraints:

$$\sum_j b_{ij}^\dagger b_{ij} = 1, \tag{A1}$$

$$e_{ij}^\dagger e_{ij} + p_{ij,i}^\dagger p_{ij,i} + p_{ij,j}^\dagger p_{ij,j} + d_{ij}^\dagger d_{ij} = 1, \tag{A2}$$

$$b_{ij}^\dagger b_{ij} = p_{ij,i}^\dagger p_{ij,i} + d_{ij}^\dagger d_{ij}. \tag{A3}$$

Now we express our Hamiltonian (16) by means of the new operators. First, the constraint term (10) is now easily written as

$$H^{\text{constr}} = \lim_{U\to\infty} U \sum_{\langle ij\rangle} d_{ij}^\dagger d_{ij} \, . \tag{A4}$$

The potential energy term (2) is straightforwardly written as

$$H^4 = -J \sum_{\langle ij\rangle} \sum_{kl} \mathrm{Re}(r_{ik} r_{jl}^*) b_{ik}^\dagger b_{ik} b_{jl}^\dagger b_{jl} \, , \tag{A5}$$

where $r_{ij} = r_j - r_i$, r_i being the complex number defining the 2D position of site i. The hopping term (4) is slightly more involved. We work in an enlarged Hilbert space and the hopping of the central ion is accompanied by a change of state of the surrounding oxygens. The corresponding expression reads

$$H^{\text{kin 1}} = -t \sum_i \sum_{jj'} b_{ij}^\dagger (d_{ij}^\dagger p_{ij,j} + p_{ij,i}^\dagger e_{ij}) \times b_{ij'} (p_{ij',j'}^\dagger d_{ij'} + e_{ij'}^\dagger p_{ij',i}) \, , \tag{A6}$$

where j, j' are both nearest neighbors of i and such that j' is the next-nearest neighbor of j.

Next, we shall treat the *oxygen* operators in the mean-field approximation, replacing them by c numbers. Before passing to the actual constrained case $U = \infty$, we consider the trivial case of $U = 0$, $J = 0$. The corresponding operator averages are obviously equal for all oxygens and we denote them as

$$\langle e^\dagger_{ij} \rangle = e, \tag{A7}$$

$$\langle p^\dagger_{ij,i} \rangle = \langle p^\dagger_{ij,j} \rangle = p, \tag{A8}$$

$$\langle d^\dagger_{ij} \rangle = d\,, \tag{A9}$$

where Eq. (A8) expresses the fact that we assume an unbroken symmetry case. The constraints (A1)–(A3) then read

$$\begin{aligned} &\sum_j \langle b^\dagger_{ij} b_{ij} \rangle = 1, \\ &e^2 + 2p^2 + d^2 = 1, \\ &\langle b^\dagger_{ij} b_{ij} \rangle = p^2 + d^2. \end{aligned} \tag{A10}$$

Since for $U = 0$ the sites are independent, the numerical values of the above averages follow just from the statistical distribution of possible mutual orientations of clock variables on neighboring sites. It is easily found that in this case $\langle b^\dagger_{ij} b_{ij} \rangle = \frac{1}{4}$, and $d^2 = \frac{1}{16}$, $p^2 = \frac{3}{16}$, $e^2 = \frac{9}{16}$. Our mean-field Hamiltonian then becomes a sum of on-site terms,

$$H^{\rm MF} = -\tilde{t} \sum_i \sum_{jj'} b^\dagger_{ij} b_{ij'}\,, \tag{A11}$$

where $\tilde{t} = tp^2(d+e)^2 = \frac{3}{16}t$. We see that in order to recover the original t we have to renormalize the mean field $\tilde{t}$ by a factor of $\frac{16}{3}$.

We can now pass to $U = \infty$, $J = 0$. Obviously, the presence of the constraint $H^{\rm constr}$ amounts to setting $d = 0$. We shall first search for an unbroken symmetry, paraelectric ground state. Following the same line of arguments as above, we have $p^2 = \frac{1}{4}$, $e^2 = \frac{1}{2}$, and we get a renormalized $\tilde{t} = \frac{2}{3}t$. This corresponds to a ground state energy per site equal to $E_g/N = -2\tilde{t} = -\frac{4}{3}t = -1.333t$, which compares very well with the result $-1.3668t$ obtained from our ground state wave function ansatz (19) (Fig. 4).

Now we show that for $U = \infty$, $J = 0$ there is also a broken symmetry, ferroelectric mean-field ground state, whose energy is degenerate with the paraelectric state found above. First of all we notice that the oxygens actually form two interpenetrating square sublattices— one formed by oxygens lying on horizontal links and other formed by those on vertical links. If we want to search for a broken symmetry solution, we have to allow for different oxygen operator averages on these two sublattices, and also the p defining Eq. (A8) may not be true anymore. Let us assume that the symmetry is broken along the horizontal axis. Then we shall have nonzero averages e_V,p_V, defined by (A7),(A8) for oxygens on links $i, j = i + \mathbf{y}$, and $e_H = \langle e^\dagger_{ij} \rangle$, $p_{H+} = \langle p^\dagger_{ij,i} \rangle$, and $p_{H-} = \langle p^\dagger_{ij,j} \rangle$ for $i, j = i + \mathbf{x}$, where $\mathbf{x}, \mathbf{y}$ are unit lattice vectors. As a consequence, the mean-field constraints (A10) will also be correspondingly generalized. Instead of (A11) we have now

$$\begin{aligned} H^{\rm MF} = -\sum_i \Big\{ &\tilde{t}_1 (b^\dagger_{i,i+\mathbf{y}} b_{i,i+\mathbf{x}} + b^\dagger_{i,i+\mathbf{x}} b_{i,i-\mathbf{y}}) \\ &+ \tilde{t}_2 (b^\dagger_{i,i-\mathbf{x}} b_{i,i+\mathbf{y}} + b^\dagger_{i,i-\mathbf{y}} b_{i,i-\mathbf{x}}) + \text{H.c.} \Big\}, \end{aligned} \tag{A12}$$

where $\tilde{t}_1 = t\, p_V\, e_V\, e_H\, p_{H+}$, $\tilde{t}_2 = t\, p_V\, e_V\, e_H\, p_{H-}$. We can now prove that $e_V = e_H = p_{H+} = \frac{1}{\sqrt{2}}$, $p_V = \frac{1}{2}$, $p_{H-} = 0$, is a self-consistent ground state solution of (A12). We get renormalized hopping parameters $\tilde{t}_1 = \frac{16}{3} t/4\sqrt{2}$, $\tilde{t}_2 = 0$, and the corresponding normalized ground state of (A12) is

$$|\Psi_g\rangle = \prod_i \left(\frac{1}{\sqrt{2}} b^\dagger_{i,i+\mathbf{x}} + \frac{1}{2} b^\dagger_{i,i+\mathbf{y}} + \frac{1}{2} b^\dagger_{i,i-\mathbf{y}} \right) |0\rangle\,. \tag{A13}$$

The self-consistency condition is easily found to be satisfied, and the solution is clearly ferroelectric. The corresponding energy per site is $E_g/N = -\sqrt{2}\tilde{t}_1 = -\frac{4}{3}t$, and therefore this state is *exactly degenerate* with the paraelectric state already found. Our mean-field theory thus predicts a critical value of $J_q/t = 0$, since the slightest positive J will make the system ferroelectric.

*Also at the International Centre for Theoretical Physics (ICTP), P.O. Box 586, 34014 Trieste, Italy.

[1] K. A. Müller and H. Burkard, Phys. Rev. B **19**, 3593 (1979).
[2] K. A. Müller, W. Berlinger, and E. Tosatti, Z. Phys. B **84**, 277 (1991).
[3] K. A. Müller, Jpn. J. Appl. Phys. Suppl. **24-2**, 89 (1985).
[4] D. Rytz, Ph.D. thesis, Ecole Polytechnique Fédérale de Lausanne, 1983.
[5] G. A. Samara, Phys. Rev. Lett. **27**, 103 (1971).
[6] R. Blinc, J. Phys. Chem. Solids **13**, 204 (1960).
[7] R. Oppermann and H. Thomas, Z. Phys. B **22**, 387 (1975).
[8] T. Schneider, H. Beck, and E. Stoll, Phys. Rev. B **13**, 1123 (1976).
[9] R. Morf, T. Schneider, and E. Stoll, Phys. Rev. B **16**, 462 (1977).
[10] J. G. Bednorz and K. A. Müller, Phys. Rev. Lett. **52**, 2289 (1984).
[11] S. Rod, F. Borsa, and J.J. van der Klink, Phys. Rev. B **38**, 2267 (1988).
[12] W. Kleemann and H. Schremmer, Phys. Rev. B **40**, 7428 (1989).
[13] M. N. Barber and W. Selke, J. Phys. A **15**, L617 (1982).
[14] Hiromoto Uwe and Tunetaro Sakudo, Phys. Rev. B **13**, 271 (1976).
[15] *Quantum Monte Carlo Methods in Equilibrium and Nonequilibrium Systems*, Proceedings of the Ninth

Taniguchi International Symposium, Susono, Japan, 1986, edited by M. Suzuki (Springer-Verlag, Berlin, 1987).
[16]A. D. Bruce and R. A. Cowley, *Structural Phase Transitions* (Taylor & Francis, London, 1981).
[17]*Structural Phase Transitions and Soft Modes*, Proceedings of the NATO Advanced Study Institute, Geilo, Norway, 1971, edited by E. J. Samuelsen, E. Andersen, and J. Feder (Universitetsforlaget Oslo, Bergen, Tromsö, 1971).
[18]J. C. Slater, J. Chem. Phys. **9**, 16 (1941).
[19]P. A. Fleury and J. M. Worlock, Phys. Rev. **174**, 613 (1968).
[20]K. Inoue, Jpn. J. Appl. Phys. **24**, Suppl. 24-2, 107 (1985).
[21]E. Courtens, G. Coddens, B. Hennion, B. Hehlen, J. Pelous, and R. Vacher, Phys. Scr. **T49B**, 430 (1993).
[22]M. Maglione, S. Rod, and U. T. Höchli, Europhys. Lett. **4**, 631 (1987).
[23]P. G. de Gennes, Solid State Commun. **1**, 132 (1963).
[24]R. J. Elliott and C. Wood, J. Phys. C **4**, 2359 (1971).
[25]P. Pfeuty, Ann. Phys. (N.Y.) **57**, 79 (1970).
[26]R. Martoňák, M. S. thesis (Magister Philosophiae) SISSA, Trieste, 1991.
[27]M. Suzuki, Prog. Theor. Phys. **37**, 770 (1967).
[28]M. A. Moore and H. C. W. L. Williams, J. Phys. C **5**, 3168 (1972).
[29]M. A. Moore and H. C. W. L. Williams, J. Phys. C **5**, 3185 (1972).
[30]M. A. Moore and H. C. W. L. Williams, J. Phys. C **5**, 3222 (1972).
[31]M. Kolb, Phys. Rev. Lett. **51**, 1696 (1983).
[32]P. Pfeuty, J. Phys. C **9**, 3993 (1976).
[33]This, incidentally, is quite a common outcome for a constrained many-body problem. For example, the well-known "non-Fermi-liquid" behavior of the 1D Hubbard model results from a very similar orthogonality catastrophe. See, e.g., P. W. Anderson, Phys. Rev. Lett. **64**, 1839 (1990).
[34]X. Y. Zhang, Elihn Abrahams, and G. Kotliar, Phys. Rev. Lett. **66**, 1236 (1990).
[35]Since bonds cannot interchange in the present model, there is no question as to their statistics, which is irrelevant. Physically, however, bonds are composite of (electron pair) + (lattice distortion), and can be thought of as bosons.
[36]J. Tobochnik, Phys. Rev. B **26**, 6201 (1982).
[37]G. Jacucci and A. Rahman, Nuovo Cimento D **4**, 341 (1984).
[38]J. Cao and B. J. Berne, J. Chem. Phys. **91**, 6359 (1989).
[39]P. Fazekas, B. Mühlschlegel, and M. Schröter, Z. Phys. B **57**, 193 (1984).
[40]This might be possible in the future, provided one can construct a suitable algorithm, built to take the constraint automatically into account, and performing some kind of collective move.
[41]G. Kotliar and A. E. Ruckenstein, Phys. Rev. Lett. **57**, 1362 (1986).